(2)

OFFICE OF NAVAL RESEARCH

Contract N00014-89-J-1497

R&T Code 413050. . .02

Technical Report No. 19

$B^+(^1S) + H_2 \rightarrow BH^+(^2\Sigma) + H$
A Woodward-Hoffmann Forbidden Ion-Molecule Reaction

by
Jeff Nichols, Samuel J. Cole, Maciej Gutowski, and Jack Simons

Prepared for Publication in

The Journal of Physical Chemistry

The University of Utah
Department of Chemistry
Salt Lake City, Utah 84112-1194

April 1991

UNCLASSIFIED

SECURITY CLASSIFICATION OF THIS PAGE

REPORT DOCUMENTATION PAGE

1a. REPORT SECURITY CLASSIFICATION UNCLASSIFIED	1b. RESTRICTIVE MARKINGS
2a. SECURITY CLASSIFICATION AUTHORITY	3. DISTRIBUTION / AVAILABILITY OF REPORT APPROVED FOR PUBLIC RELEASE: DISTRIBUTION UNLIMITED
2b. DECLASSIFICATION / DOWNGRADING SCHEDULE	
4. PERFORMING ORGANIZATION REPORT NUMBER(S) ONR TECHNICAL REPORT # 19	5. MONITORING ORGANIZATION REPORT NUMBER(S)
6a. NAME OF PERFORMING ORGANIZATION THE UNIVERSITY OF UTAH 6b. OFFICE SYMBOL (If applicable)	7a. NAME OF MONITORING ORGANIZATION OFFICE OF NAVAL RESEARCH CHEMISTRY PROGRAM
6c. ADDRESS (City, State, and ZIP Code) DEPARTMENT OF CHEMISTRY UNIVERSITY OF UTAH SALT LAKE CITY, UT 84112	7b. ADDRESS (City, State, and ZIP Code) 800 NO. QUINCY ST. ARLINGTON, VA 22217-5000
8a. NAME OF FUNDING / SPONSORING ORGANIZATION OFFICE OF NAVAL RESEARCH 8b. OFFICE SYMBOL (If applicable) ONR	9. PROCUREMENT INSTRUMENT IDENTIFICATION NUMBER N00014-89-J-1497
8c. ADDRESS (City, State, and ZIP Code) 800 NO. QUINCY ST. ARLINGTON, VA 22217	10. SOURCE OF FUNDING NUMBERS PROGRAM ELEMENT NO. / PROJECT NO. / TASK NO. / WORK UNIT ACCESSION NO

11. TITLE (Include Security Classification)
B + (^{1}S) + H_2 - BH^+(^{2}Sigma) + H A Woodward-Hoffmann Forbidden Ion-Molecule Reaction

12. PERSONAL AUTHOR(S)
Jeff Nichols, Samuel J. Cole, Maciej Gutowski, and Jack Simons

13a. TYPE OF REPORT	13b. TIME COVERED	14. DATE OF REPORT (Year, Month, Day)	15. PAGE COUNT
TECHNICAL	FROM 12/90 TO 3/91	April 17, 1991	

16. SUPPLEMENTARY NOTATION

17. COSATI CODES			18. SUBJECT TERMS (Continue on reverse if necessary and identify by block number)
FIELD	GROUP	SUB-GROUP	

19. ABSTRACT

The reaction of $B^+(^1S)$ with H_2 on the ground potential energy surface is examined using *ab initio* electronic structure methods. A weakly bound T-shaped $B^+\cdots H_2$ complex of C_{2v} symmetry is found to lie 855 cm^{-1} below the $B^+ + H_2$ reactant energy. Its H-H internuclear distance is only slightly distorted from that of H_2; the B-H distance (ca. 2.6 Å) is much longer than the covalent bond length in BH^+ (1.2 Å). Further along the reaction coordinate is found a narrow 'entrance valley' characterized by strong B^+-to-H_2 inter-reactant forces but very small distortion of the H-H bond length or the H-H vibrational frequency. As one proceeds further up this valley, a geometry is reached at which the asymmetric distortion mode (of b_2 symmetry) develops negative curvature. Distortion along the asymmetric mode leads to a transition state of C_s symmetry posessing one 'long' B-H distance (r_{BH}= 1.765 Å), one 'short' B-H distance (r_{BH}' = 1.251 Å) and an essentially 'broken' H-H bond (r_{HH} = 1.516 Å). Its energy lies 22,528 cm^{-1} above $B^+ + H_2$ and 2031 cm^{-1} or ca. 0.25 eV above the thermodynamic reaction threshold for $BH^+ + H$ formation, which is predicted to be endoergic by 20,497cm^{-1}. A geometrically stable linear $HBH^+(^1\Sigma)$ species is found to lie 19,259 cm^{-1} below $B^+ + H_2$. Its BH bond length (r_{BH}=1.173 Å) is only slightly longer than that in BH^+ (1.2 Å). Similarities and differences among reactions of the isoelectronic Be, B^+, and Li^- with H_2 are also discussed.

20. DISTRIBUTION / AVAILABILITY OF ABSTRACT	21. ABSTRACT SECURITY CLASSIFICATION
☒ UNCLASSIFIED/UNLIMITED ☐ SAME AS RPT ☐ DTIC USERS	UNCLASSIFIED
22a. NAME OF RESPONSIBLE INDIVIDUAL PROFESSOR JACK SIMONS	22b. TELEPHONE (Include Area Code) (801) 581-8023
	22c. OFFICE SYMBOL

DD FORM 1473, 84 MAR 83 APR edition may be used until exhausted. All other editions are obsolete.

SECURITY CLASSIFICATION OF THIS PAGE

$B^+(^1S) + H_2 \Longrightarrow BH^+(^2\Sigma) + H$

A Woodward-Hoffmann Forbidden Ion-Molecule Reaction

Jeff Nichols#, Samuel J. Cole+, Maciej Gutowski, and Jack Simons
Chemistry Department
University of Utah
Salt Lake City, Utah 84112

Abstract

The reaction of $B^+(^1S)$ with H_2 on the ground potential energy surface is examined using *ab initio* electronic structure methods. A weakly bound T-shaped $B^+\cdots H_2$ complex of C_{2v} symmetry is found to lie 855 cm^{-1} below the $B^+ + H_2$ reactant energy. Its H-H internuclear distance is only slightly distorted from that of H_2; the B-H distance (ca. 2.6 Å) is much longer than the covalent bond length in BH^+ (1.2 Å). Further along the reaction coordinate is found a narrow 'entrance valley' characterized by strong B^+-to-H_2 inter-reactant forces but very small distortion of the H-H bond length or the H-H vibrational frequency. As one proceeds further up this valley, a geometry is reached at which the asymmetric distortion mode (of b_2 symmetry) develops negative curvature. Distortion along the asymmetric mode leads to a transition state of C_s symmetry posessing one 'long' B-H distance (r_{BH}= 1.765 Å), one 'short' B-H distance ($r_{BH'}$ = 1.251 Å) and an essentially 'broken' H-H bond (r_{HH} = 1.516 Å). Its energy lies 22,528 cm^{-1} above $B^+ + H_2$ and 2031 cm^{-1} or ca. 0.25 eV above the thermodynamic reaction threshold for $BH^+ + H$ formation, which is predicted to be endoergic by 20,497cm^{-1}. A geometrically stable linear $HBH^+(^1\Sigma)$ species is found to lie 19,259 cm^{-1} below $B^+ + H_2$. Its BH bond length (r_{BH}=1.173 Å) is only slightly longer than that in BH^+ (1.2 Å). Similarities and differences among reactions of the isoelectronic Be, B^+, and Li^- with H_2 are also discussed.

#Utah Supercomputer Institute/IBM Corporation Partnership, Salt Lake City, Utah 84112
Permanent address: CAChe™ Group, Tektronix, Inc., P.O. Box 500 M.S. 13-400, Beaverton, OR 97077.

I. Introduction

Earlier theoretical calculations[1] on $Be(^1S) + H_2 \Longrightarrow HBeH(^1\Sigma)$ and on[2] $Mg(^1S) + H_2 \Longrightarrow HMgH(^1\Sigma)$ yielded qualitatively similar ground-state, C_{2v} - constrained potential energy surfaces. A two-dimensional contour characterization of such C_{2v} - constrained potential energy surfaces is given in Fig. 1. Both of these alkaline earth atoms, as well as the analogous B^+ ion considered here, have $ns^2\ ^1S$ ground electronic states and relatively low-lying nsnp $^{1,3}P$ excited states. As discussed in detail below, the chemical reactivity of the ^1S ground-states of such species is strongly influenced by the presence of the excited $^{1,3}P$ states. Before discussing our motivations for undertaking the theoretical study of the $B^+(^1S) + H_2 \Longrightarrow BH^+(^2\Sigma) + H$ reaction and our findings, let us exploit our experience on the Be and Mg reactions to anticipate some of the electronic structure characteristics that would be expected to affect strongly the dynamics[3a,3b,3c] (e.g., energy threshold, cross-section magnitude, and energy dependence) of the $B^+ + H_2$ reaction.

A. The Electronic Configurations of Interest in C_{2v} Symmetry

1. The $M + H_2$ Reactant and HMH Product Configurations

Briefly, the ns^2 configuration of the reactant M atom (or ion) when combined with the σ^2_g configuration of the H_2 molecule in its $X\ ^1\Sigma_g$ ground state, does not correlate with the ground-state $\sigma^2_g\ \sigma^2_u$ configuration of the linear HMH molecule (or ion). In C_{2v} symmetry, the $M + H_2$ reactants have the $ns^2\ \sigma^2_g = 1a^2_1 2a^2_1$ electronic configuration, and the HMH products have the $\sigma^2_g\ \sigma^2_u = 1a^2_1 1b^2_2$ configuration. Moreover, neither of these two configurations can describe the MH + H products which require an 'open-shell' configuration of the form $\sigma^2_{MH}\ \sigma_M\ \sigma_H$. For the $M + H_2$ reactants, the labels $1a_1$, $2a_1$, and $1b_2$ are used to denote the valence M ns, $H_2\ \sigma_g$, and M (in plane) np orbitals. The M inner-shell orbitals are not explicitly identified in this abbreviated notation. For the HMH product molecule, $1a_1$, $2a_1$, and $1b_2$ denote the M-H σ, σ^*, and σ orbitals, respectively. For the MH + H products, σ_{MH} labels the M-H bonding σ orbital, σ_M the M-centered non-bonding orbital, and σ_H the H-atom 1s orbital.

Both of the above dominant configurations of the $M + H_2$ reactant and MH_2 product are of $^1A_1$ symmetry, so they mix as one proceeds along the reaction path to produce the 'avoided crossing' which gives rise to the well known symmetry imposed activation barrier characteristic of such Woodward-Hoffmann forbidden reactions. For a C_{2v} symmetry preserving reaction path appropriate to the insertion of B^+ into H_2 to produce HBH^+, these correlations are described semi-quantitavely in Fig. 2.

2. Low-Energy Excited State Configurations

The excited $^{1,3}P$ states of the M species, when interacting with H_2 in C_{2v} symmetry, give rise to singlet and triplet states of A_1, B_1, and B_2 symmetry. The $^{1,3}B_2$ states posesses the most attractive interactions because they allow M's in-plane np orbital of b_2 symmetry to interact constructively with the H_2 molecule's 'empty' antibonding σ_u orbital as shown in Fig. 3. The relative locations of these $^{1,3}B_2$ states along the insertion reaction's C_{2v} reaction path are also depicted in Fig. 2 (with the triplet states lying below the singlets).

B. Implications for Reactivity

The fact that the $^1A_1$ ground state surface is either intersected or closely approached by the $^{1,3}B_2$ surfaces has important consequences for the insertion reaction under discussion. In particular, collsions entering the region where the $^1A_1$ and $^1B_2$ surfaces are close in energy may 'hop' from the ns^2 $^1A_1$ entrance-channel surface to the $^1B_2$ surface if the collision occurs with some degree of assymmetry. Collisions that occur slightly away from C_{2v} symmetry will experience weak coupling of the $^1A_1$ and $^1B_2$ surfaces (which are both of $^1A'$ symmetry in the lower C_s point group). The point is that any loss of C_{2v} symmetry permits the $^1A_1$ and $^1B_2$ states to mix, thereby allowing reactants to move onto the $^1B_2$ surface, which, in C_s symmetry, correlates to MH ($^2\Sigma$) + H products. Of course, if any appreciable spin-orbit coupling is operative, transitions to the $^3B_2$ surface. which also correlates directly to the MH ($^2\Sigma$) + H products, can also occur. It is through such surface 'hoppings' that the MH + H channel is accessed when the reaction begins with ground-state M and H_2 species.

C. Reaction Path "Shape'

A somewhat more quantitative view of the C_{2v} ground-state energy surface appropriate to these 'insertion' reactions is provided by Fig. 1 for the *ab initio* calculated[1] $^1A_1$ surface of Be(^1S) + H_2 ==> HBeH (X $^1\Sigma_g$). This surface and others of this M (ns^2; ^1S) + H_2 ==> HMH ($^1\Sigma_g$) family are characterized by potential energy landscapes along which:

a. The M + H_2 entrance channel is very 'straight' (i.e., the reaction coordinate is dominated by M-to-H_2 relative motion with very little H-H displacement) and has very large positive curvature transverse to the reaction coordinate (i.e., the H-H bond remains intact and is very 'stiff').
b. Once a critical M-to-H_2 distance is reached, the reaction coordinate undergoes a sudden change to become dominated by H-H stretching with much less M-to-H_2 movement.
c. Further along the reaction path, a C_{2v} transition state is reached that lies more than 2 eV above[1] the energy of the M + H_2 reactants and even above the energy of the MH + H fragments that could be formed if C_{2v} symmetry were not (artificially) enforced.
d. Between the point where the reaction path acquires negative curvature along its 'uphill' coordinate and the C_{2v} - constrained transition state, a region appears within which negative curvature also exists along the asymmetric (b_2) distortion. Because of the constraint to C_{2v} symmetry, the force (i.e., teh energy gradient) along this b_2 direction vanishes identically. The appearance of negative curvature along a direction transverse to the reaction cocrdinate indicates that a lower-energy path can be found if

one moves away from the C_{2v} geometry along this asymmetric direction. In the above cases, doing so eventually leads to formation of ground-state MH + H products. The negative curvature on the $^1A_1$ surface along the b_2 direction is a signal that a $^1B_2$ surface is in close proximity; it does not mean that an intersection with a $^1B_2$ surface is taking place, but that such a surface is energetically nearby. It is in this region of the surface that one must break C_{2v} symmetry in search of the true, lowest-energy, transition state.

e. If C_{2v} symmetry constraints are kept operative, movement along the b_2 asymmetric mode will not occur, and the reaction coordinate will evolve smoothly to and beyond the C_{2v} - constrained transition state mentioned above.

f. Beyond this C_{2v} transition state, the reaction coordinate eventually develops positive curvature as the linear HMH($^1\Sigma_g$) geometry is approached.

D. Why Study $B^+(^1S) + H_2$?

The present work is aimed at extending the investigations described above in at least two aspects: (i) to include a positive metal ion (but still with a closed-shell ^1S ground electronic state) as the reactive species so any effects caused by ion-molecule interactions can be examined, and (ii) to investigate reaction paths that are not C_{2v} - preserving so as to permit the MH + H product channel to be explored. We chose $B^+(^1S)$ as the positive ion because: (i) it is isoelectronic with $Be(^1S)$ which we examined earlier (and thus similarities and differences between the Be and B^+ cases are of interest), (ii) it allows highly accurate calculations to be performed with reasonable effort, and (iii) experimental guided ion beam and other data[3a,3d] giving the cross-section for BH^+ production as a function of B^+ kinetic energy are available and in need of theoretical interpretation.

II. Computational Methods

A. Basis Sets

The basis set for the H atoms consists of the Dunning augmented correlation consistent (cc) polarized valence triple-zeta (p-VTZ) [5s2p1d| 3s2p1d] set[4] of functions. For the B^+ ion, the Dunning [10s5p2d| 4s3p2d] augmented cc p-VTZ basis set was used. A total of 55 contracted Gaussian-type basis functions resulted.

B. Electronic Configurations and Wavefunctions

Both multiconfigurational self-consistent field (MCSCF) and coupled-cluster methods were used to treat correlations among the four valence electrons of the BHH^+ system. In particular, the CCSD(T) variant[5] of the coupled-cluster approach[6], which includes all single and double excitations in a fully correct manner and treats triple excitations by approximate non-iterative means, was employed.

The discussion of Sec. I makes it clear that no single electronic configuration can describe even the ground state of this system throughout the C_{2v} or C_s reaction paths. For this reason, multiconfigurational methods were required. In the MCSCF calculations, the four valence electrons were distributed, in all ways consistent with overall spatial and spin symmetry, among 6 valence orbitals. In the C_{2v} calculations, 4 of these orbitals were of a_1 symmetry, 1 was of b_2 symmetry, and 1 was of b_1 symmetry. In C_s symmetry, there were 5 of a' symmetry and 1 of a" symmetry. The two B^+ 1s electrons

were constrained to occupy a single a_1 or a' core orbital in all of the electronic configurations generated. This process generated 41 electronic configurations of $^1A_1$ symmetry in the C_{2v} point group and 65 of $^1A'$ symmetry in the C_s point group.

The above MCSCF calculations were employed, along with our Utah MESSKit[7] analytical energy derivative and potential energy surface 'walking' algorithms[8] to find and characterize (via geometry and local harmonic vibrational frequencies) the local minima, transition states, and reaction paths discussed below. Near each such point, the CCSD(T) method was used to evaluate the total correlation energies at a more accurate level; finite difference methods were also employed within the CCSD(T) approach to refine the predicted geometry of each such point on the surface.

III. Findings and Comparison to Guided Ion Beam Results

As detailed in Table I and described qualitatively in Figs. 2 and 4, we find the potential energy surface for $B^+(^1S) + H_2 \Longrightarrow BH^+(^2\Sigma) + H$ to possess most of the features that are expected from the discussion in Sec. I. Although there are differences that might have been expected because of the additional long-range ion-molecule interactions that are operative in this case, we find such affects to be quite small in this case. Our primary findings are summarized as follows:

a. A weakly bound $B^+\cdots H_2$ complex lies 1143 cm^{-1} below the $B^+ + H_2$ reactant energy. When zero-point corrected, this complex is stable by only 855 cm^{-1}. The complex has a triangular C_{2v} equilibrium structure in which the H-H internuclear distance is only slightly distorted from that of H_2; the B-H distance (ca. 2.6 Å) is much longer than the covalent bond length in BH^+ (1.2 Å). Further along the reaction coordinate, one finds a 'straight and narrow' reaction path characterized by stronger and stronger B^+-to-H_2 inter-reactant forces but very small distortion of the H-H bond length or the H-H vibrational frequency. The very restricted range of geometries (i.e., the narrowness) of this entrance channel and its lack of 'curvature' coupling B^+-to-H_2 translational energy to H-H vibrational energy would be expected to produce clear signatures in the $B^+ + H_2 \Longrightarrow BH^+ + H$ experimental data.

b. As the B^+ ion approaches the H_2 molecule from very long range (e.g., R= 25 Å or further), the charge-quadupole interaction (which varies as R^{-3}) favors the 'T-shaped' C_{2v} approach which eventually produces the above straight and narrow reaction path. The permanent quadupole moment of H_2 attracts positive ions to the internuclear regions and repels positive ions from positions along the H-H axis at long range. As one moves to smaller R values, the charge-induced dipole interaction (which varies as R^{-4}) comes into play. This factor favors approach of a positive (or negative) ion along the H-H axis (because $\alpha_{||} = 0.934$ Å$^3 > \alpha_{\perp} = 0.718$ Å^3). Although these electrostatic and induced interactions are dominant at very long range, we find that by the time the B^+ is close enough to the H_2 moleucle to experience interaction energies of the order of a few kcal/mol, the energetically favored approach corresponds to a T-shaped C_{2v} structure. Although a colinear approach path may have been expected to be more favorable for larger R values, we find that the linear structure becomes unstable with respect to bending distortion even at rather large R values. As a result, the reaction path 'bends' toward the C_{2v} path which it then follows throughout the remainder of the B^+ to H_2 approach.

c. The $B^+ + H_2$ ==> $BH^+ + H$ reaction is predicted to be endoergic by 21,318cm^{-1} (20,497 cm^{-1} when zero-point corrected). In the guided ion beam experiments[3a], no flux of BH^+ product ions are detected when B^+ ions collide with H_2 with kinetic energies at or slightly above this threshold; this has been used to infer that an additional activation barrier is present.

d. As one proceeds along the straight and narrow entrance channel starting from the $B^+ + H_2$ species (along which C_{2v} symmetry obtains even though not enforced), a geometry is reached at which the asymmetric distortion mode (of b_2 symmetry) develops negative curvature. This occurs at an energy of -25.341096 Hartree, 23,100 cm^{-1} above the $B^+ + H_2$ reactants; the geometry where this occurs has an HH distance of 1.305 Å and a BH distance of 1.481 Å. From here, distortion along the asymmetric mode leads to a transition state that lies below the C_{2v} - constrained transition state. The resulting C_s transition state structure posesses one 'long' B-H distance (r_{BH}= 1.765 Å), one 'short' B-H distance ($r_{BH'}$ = 1.251 Å) and an essentially 'broken' H-H bond (r_{HH} = 1.516 Å). Its energy is 23,518 cm^{-1} above the $B^+ + H_2$ asymptote; when zero-point corrected, this point lies 22,528 cm^{-1} above $B^+ + H_2$. This critical point lies 2031 cm^{-1} or ca. 0.25 eV above the thermodynamic reaction threshold. This energy gap corresponds approximately to where the guided ion beam experiments first detect production of BH^+ product ions.

e. A geometrically stable linear $HBH^+(^1\Sigma)$ species is found to lie 20,892 cm^{-1} (19,259 cm^{-1} when zero-point corrected) below $B^+ + H_2$. This species lies on the ground state $^1A_1$ potential energy surface and correlates with the $B^+(^1S) + H_2$ reactants when C_{2v} symmetry is enforced. Its BH bond length (r_{BH}=1.173 Å) is only slightly longer than that in BH^+ (1.2 Å).

f. In the absence of enforced C_{2v} symmetry, the $^1A_1$ and $^1B_2$ surfaces of Fig. 2 are of the same ($^1A'$) symmetry, and can therefore couple to produce 'avoided crossings'. As a result of these interactions, the ground-state $B^+(^1S) + H_2$ reactants can now correlate directly to the $BH^+(^2\Sigma) + H$ products as summarized in the C_s - symmety correlation diagram of Fig. 4.

IV. Discussion of Results and Summary

Many of the features observed for the $B^+ + H_2$ surface(s) are remarkably similar to those found earlier for Be + H_2. In Fig. 5 we summarize the relative energies of the reactants, transition states, and products that arise in these two systems; in both cases, all energies are defined relative to the ground state of the M + H_2 reactants.

The energy of the $BeH_2^{\#}$ transition state corresponds to C_{2v} symmetry although C_s symmetry was explored in these earlier calculations. As Be approaches H_2, the reaction path preserves C_{2v} symmetry and leads to the transition state shown in Fig. 5, at which the curvature along the asymmetric b_2 distortion mode is positive. Past this transition state, along the way to the linear HBeH geometry, a state of $^1B_2$ symmetry crosses the $^1A_1$ surface. At this point, the curvature along the b_2 mode is negative. As a

result, the reaction path moves away from C_{2v} symmetry and produces BeH + H products.

It may be somewhat surprising that, although the ^3P and ^1P excited states of B^+ lie considerably higher than the corresponding $^{3,1}P$ states of Be (because of the higher nuclear charge of B^+), the relative energies of the transition states, MH + H, and HMH species are rather similar. It should be noted that, because the $^{1,3}P$ states of B^+ lie considerably higher than those of Be, the intersections of the resultant $^{1,3}B_2$ states with the $^1A_1$ ground state are somewhat different for B^+ and Be. In particular, both of the $^{1,3}B_2$ states of BeH_2 intersect the $^1A_1$ state near the C_{2v} transition state. However, it appears that the $^1B_2$ state of BH_2^+ does not intersect the $^1A_1$ state as one proceeds along the reaction path toward the transition state (although it certainly couples strongly to it to produce the negative curvature along the b_2 mode).

To explore such differences and similarities further, it is interesting to speculate about another isoelectronic system: $Li^- + H_2 \Longrightarrow LiH^- + H$, $HLiH^-$. Using the known[9] electron affinities of Li and of LiH, as well as the LiH and H_2 bond energies, one finds that $LiH^- + H$ should lie 19,100 cm^{-1} above $Li^- + H_2$. This energy difference is remarkably close to those for $B^+ + H_2 \Longrightarrow BH^+ + H$ and $Be + H_2 \Longrightarrow BeH + H$. The energies of the $HLiH^-$ species and of the C_{2v} or C_s transition states for the $Li^- + H_2$ reaction are not yet known, so further comparisons can not be made.

Major differences between the Li^- case and those for B^+ and Be involve the location of the $^{3,1}P$ excited states. For B^+ and Be, the lowest of these states, the ^3P state, lies 37,300 cm^{-1} and 22,000 cm^{-1}, respectively, above the ^1S ground state. For Li^-, the ^3P state lies higher in energy than Li (plus a free electron) and hence is metastable with respect to autodetachment. In particular, the ^3P and ^1P states are believed to lie between 5000 and 10,000 cm^{-1} and between 12,000 and 13,000 cm^{-1} above the ^1S state, while the Li^- electron detachment energy is only 5000 cm^{-1}. For these reasons, the intersection of the $^1A_1$ ground state C_{2v} surface for $Li^- + H_2$ by the excited $^1B_2$ surface is expected to occur at much lower energy than in the B^+ and Be cases. Moreover, the $^2A_1$ surface corresponding to the autodetached $Li + H_2$ species is also expected to come into play at low collision energies. Therefore, qualitatively different behavior is expected both in the low-energy potential surfaces of $Li^- + H_2$ and in the guided ion beam experiments studying Li^- collisions with H_2 . It is our intention to explore this interesting case in the near future.

Before closing, it should be mentioned that there are interesting aspects of the $B^+ + H_2$ potential energy surfaces that were not addressed here because of our emphasis on the lowest singlet-state potential. In particular, the location of the $^3B_2$ surface in the neighborhood of the singlet state's C_s transition state is of substantial importance to a full interpretation of the $B^+ + H_2$ reactivity data. If transitions to the $^1B_2$ surface play an important role, transitions to the corresponding triplet surface will also be operative. The latter events may occur with reduced probability because of the need for singlet-triplet coupling, but they will occur at lower energy because the $^3B_2$ state lies below the $^1B_2$ state.

Finally, in this work emphasis has been placed on the reaction path as it enters the 'straight and narrow' channel of C_{2v} symmetry; little has been said of colinear M-HH geometries. Hurst has shown that the linear approach does not lead to a lower-energy

path to the formation of $BH^+(^2\Sigma)$ + H, and our data confirms that the energetically favored approach evolves into the C_{2v} geometry once the B^+ and H_2 begin to interact via chemical valence forces.

Acknowledgments

This work was supported in part by the Office of Naval Research and by NSF Grant #CHE8814765. We acknowledge our colleague, Prof. P. B. Armentrout, for stimulating our interest in this particular system. We thank the Utah Supercomputer Institute for staff and computer resources.

References:

1. D. O'Neal, H. Taylor, and J. Simons, J. Phys. Chem. 88, 1510 (1984).

2. N. Adams, W. H. Breckenridge, and J. Simons, Chem. Phys. 56, 327 (1981).

3a. P. B. Armentrout, Inter. Rev. Phys. Chem. 9, 115 (1990); J. L. Elkind and P. B. Armentrout (unpublished results); S. A. Ruatta, L. Hanley, and S. L. Anderson, J. Chem. Phys. 91, 226 (1989);
3b. P. Rosmus and R. Klein, Thesis by Klein, University of Frankfurt (1984).
3c. F. Schneider, L. Zülicke, R. Polak, and J. Vojtik, Chem. Phys. Letts. 105, 608 (1984).
3d. K. C. Lin, H. P. Watkins, R. J. Cotter, and W. S. Koski, J. Chem. Phys. 56, 1003 (1974); S. A. Ruatta, L. Hanley, and S. L. Anderson, J. Chem. Phys. 91, 226 (1989).

4. T. Dunning, J. Chem. Phys. 90, 1007 (1989).

5. K. Raghavachari, G. W. Trucks, J. A. Pople, and M. Head-Gordon, Chem.Phys. Lett., 157, 479 (1989).

6. J. Cizek, J. Chem. Phys. 45, 4256 (1966); Advan. Chem. Phys. 14, 35 (1969). J. Cizek, and J. Paldus, Intern. J. Quantum Chem. 5, 359 (1971). R. J. Bartlett, J. Phys. Chem., 93, 1697 (1989) for a recent comprehensive review of developments in this field.

7. The Utah MESS-KIT is a suite of highly modular codes that were programmed in-house to give a variety of electronic structure functionalities by J.A. Nichols, M.R. Hoffmann, R.A. Kendall, H.L. Taylor, D.W. O'Neal, E. Earl, R. Hernandez, M. Gutowski, J.Boatz, K. Bak, J. Anchell, X. Wang, M. Feyereisen, and J. Simons.

8. J. Nichols, H. Taylor, P. Schmidt and J. Simons, J. Chem. Phys. 92, 340 (1990); J. Simons, P. Jørgensen, H. Taylor, and J. Ozment, J. Phys. Chem. 87, 2745 (1983); D. O'Neal, H. Taylor, and J. Simons, J. Phys. Chem. 88, 1510 (1984); A. Banerjee, N. Adams, J. Simons, and R. Shepard, J. Phys. Chem. 89, 52 (1985); H. Taylor and J. Simons, J. Phys. Chem. 89, 684 (1985); C. J. Cerjan and W. H. Miller, J. Chem. Phys., 75, 2800 (1981); J. Baker, J. Comp. Chem. 9(5), 465 (1988); J. Baker, J. Comp. Chem. 7(4), 385 (1986).

9. The EA of Li is 0.62 eV (H. Hotop and W. C. Lineberger, J. Phys. Chem. Ref. Data, 14, 731 (1985); the EA of LiH is 0.3 eV (K. M. Griffing, J. Kenney, J. Simons, and K. D. Jordan, J. Chem. Phys. 63, 4073 (1975).

10. D. M. Hurst, Chem. Phys. Letters 95, 591 (1983).

Table I. Total and Relative Energies, Geometries, and Vibrational Frequencies for Species Along the $B^+ + H_2 \Longrightarrow BH^+ + H$ Reaction Path[a]

Species	Method Used	Electronic Energy (Hartrees)	Optimized Geometry (Å)	MCSCF Frequencies[c]/ Zero Point Energies (cm^{-1})	Relative Energies (cm^{-1})[b]
$B^+(^1S) + H_2$	MCSCF CCSD(T)	-25.446357 -25.468865	r_{HH} = 0.755 r_{HH} = 0.734	4224/2112	0
BH_2^+ C_{2v} complex	MCSCF CCSD(T)	-25.468239 -25.474069	r_{HH} = 0.762; r_{BH}= 2.605 r_{HH} = 0.743; r_{BH}= 2.605	230 (a_1), 437 (b_2), 4133 (a_1)/ 2400	-1143
BH_2^+ C_{2v} transition state	MCSCF CCSD(T)	-25.322627 -25.352230	r_{HH} = 1.396; r_{BH}= 1.411	4512i (a_1), 1279 (a_1), 3424i (b_2)[d]	25,595
$HBH^+(^1\Sigma)$	MCSCF CCSD(T) CCSD(T)	-25.524859 -25.563931 -25.564067	r_{BH}= 1.183 $r_{BH'}$ = 1.172 r_{BH}=1.173	2911 (a_1), 2632 (b_2), 973 (bending)/ 3745	-20,892
BH_2^+ C_s transition state	MCSCF CCSD(T)	-25.332540 -25.361695	r_{HH} = 1.516 r_{BH}= 1.765 $r_{BH'}$ = 1.251	2840i,small[e], 2087/ ca. 1050	23,518
$BH^+(^2\Sigma)$ + H	MCSCF CCSD(T)	-25.351373 -25.371722	r_{BH} = 1.199 r_{BH} = 1.198	2582/ 1291	21,318
BHH^+ linear complex	MCSCF CCSD(T) CCSD(T)	-25.446663 -25.469942 -25.488630	r_{HH} = 0.756 r_{BH}= 2.729 r_{HH} = 0.702 r_{BH} = 2.865	112, 4202, 303i (bending)[d] /2157	-4337

a. Where separate geometry optimizations were carried out at the MCSCF and CCSD(T) levels, two sets of geometries are reported. In all cases, the MCSCF geometry is listed first, and the CCSD(T) geometry appears second. Where geometry optimization could not be carried out at the CCSD(T) level, the CCSD(T) energies were computed at the MCSCF geometries.

b. In all cases, only the CCSD(T) energies are used because they represent our best values. They are given relative to the $B^+ + H_2$ reactants. These are electronic energies, and thus do not include zero-point corrections.

c. These local harmonic frequencies were obtained from the analytical second derivatives of the MCSCF energy at the MCSCF geometries.

d. It is not appropriate to compute zero point energies here because this is neither a true minimum nor transition state (i.e., more than one imaginary frequency appears).

e. The precise location of the C_s transition state was very difficult to determine. See text for further discussion.

Figure Captions

Figure 1. Two-dimensional contour plot of the ground-state $^1A_1$ potential energy surface for the C_{2v} insertion of Be(^1S) into H_2 to produce linear HBeH($^1\Sigma$). The contour spacings represent approximately 5,000 cm^{-1} in energy. The labels a-d, f refer to the geometrical points discussed in Sec. I.C. Along the vertical axis is the distance from the B^+ to the center of the H-H bond; the horizontal axis labels the H-H distance.

Figure 2. Configuration correlation diagram for C_{2v} insertion of $B^+(^1S)$ into H_2 to produce linear HBH^+. The energies are in untis of 1000 cm^{-1}. The $1a_1$, $2a_1$, and $1b_2$ orbitals correspond to the H_2 σ_g, B^+ 2s, and B^+ 2p (in plane) orbitals, respectively for the $B^+ + H_2$ reactants. For the HBH^+ product, the $1a_1$ and $1b_2$ orbitals are the two (symmetric and assymmetric) σ B-H bonding orbitals.

Figure 3. Constructive interaction between the in-plane M np orbital of b_2 symmetry and the antibonding H_2 σ_u orbital also of b_2 symmetry.

Figure 4. Configuration correlation diagram for C_s insertion of $B^+(^1S)$ into H_2 to produce either linear HBH^+ or $BH^+(^2S)$ + H. The energies are in units of 1000 cm^{-1}. The 1a', 2a', and 3a' orbitals correspond to the H_2 σ_g, B^+ 2s, and B^+ 2p (in plane) orbitals, respectively for the $B^+ + H_2$ reactants. For the HBH^+ product, the 1a' and 3a' orbitals are the two (symmetric and assymmetric) σ B-H bonding orbitals. For BH^+ + H, 1a' is the BH^+ σ bonding orbital, 3a' is the BH^+ non-bonding σ orbital, and 2a' is the H atom 1s orbital.

Figure 5. Energy diagram showing relative energies of M + H_2, HMH, MH + H, and transition states for the $B^+ + H_2$ and Be + H_2 cases. Also shown are the locations of the $^{1,3}P$ excited states of the B^+ and Be species. All energies are in untis of 1000 cm^{-1}.

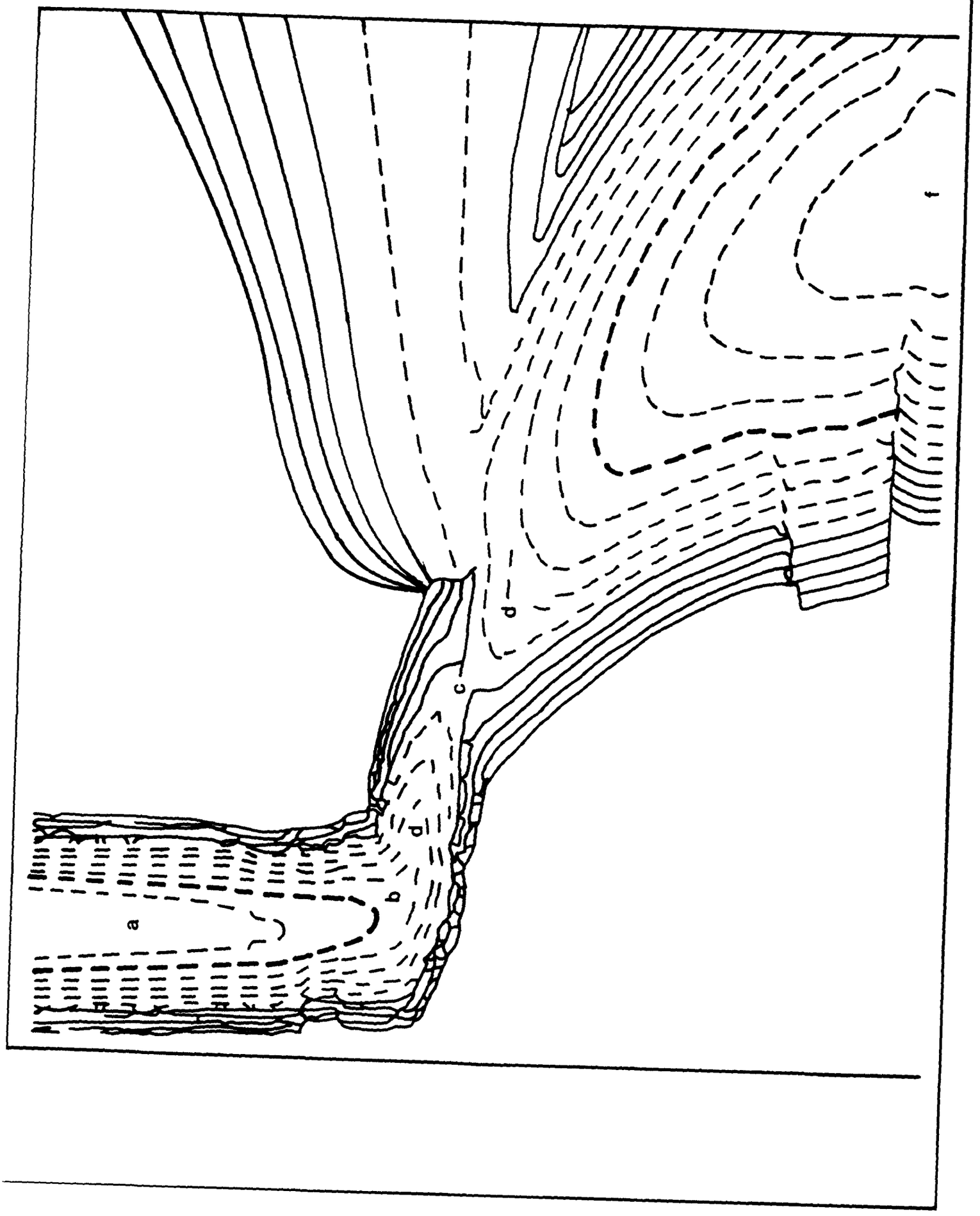
a
b
c
d
e
f

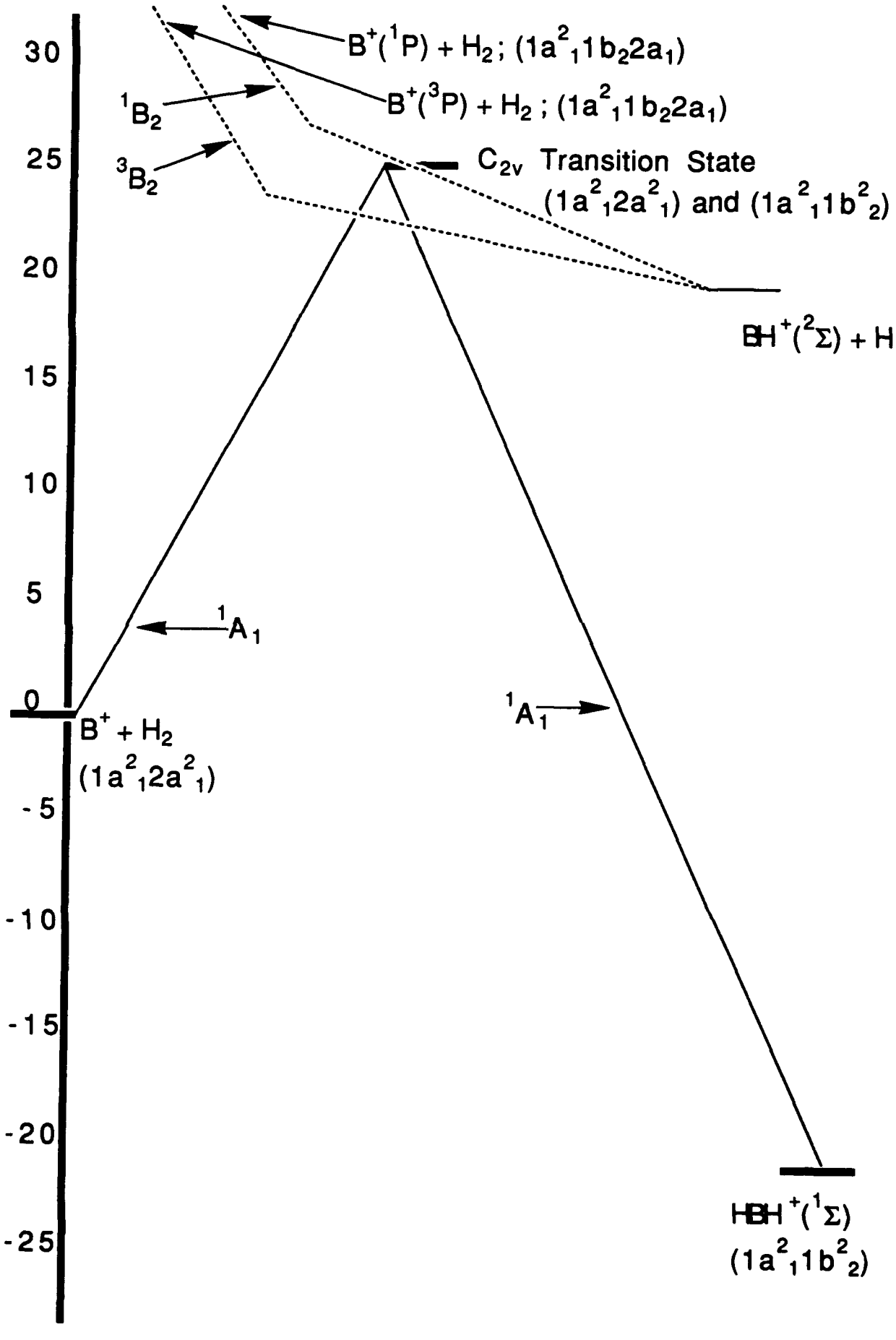
30
25
20
15
10
5
0
-5
-10
-15
-20
-25
$B^+(^1P) + H_2$; $(1a^2_1 1b_2 2a_1)$
$B^+(^3P) + H_2$; $(1a^2_1 1b_2 2a_1)$
$^1B_2$
$^3B_2$
C_{2v} Transition State
$(1a^2_1 2a^2_1)$ and $(1a^2_1 1b^2_2)$
$BH^+(^2\Sigma) + H$
$^1A_1$
$^1A_1$
$B^+ + H_2$
$(1a^2_1 2a^2_1)$
$HBH^+(^1\Sigma)$
$(1a^2_1 1b^2_2)$

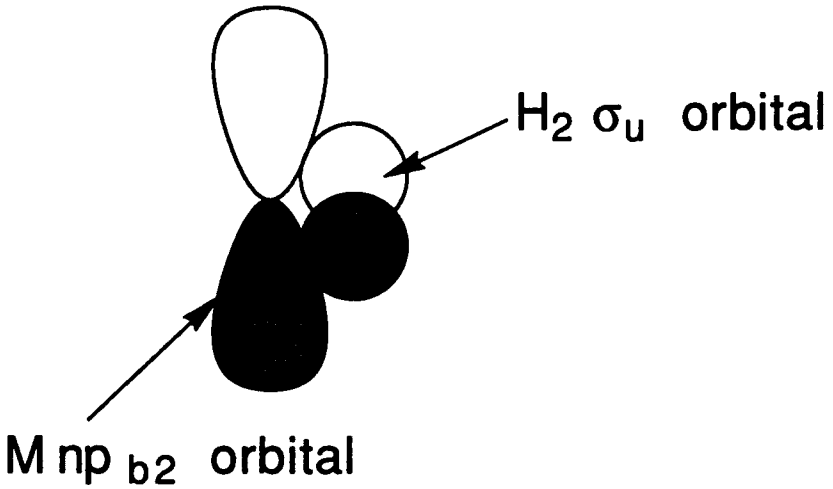
$H_2\ \sigma_u$ orbital
M np $_{b2}$ orbital

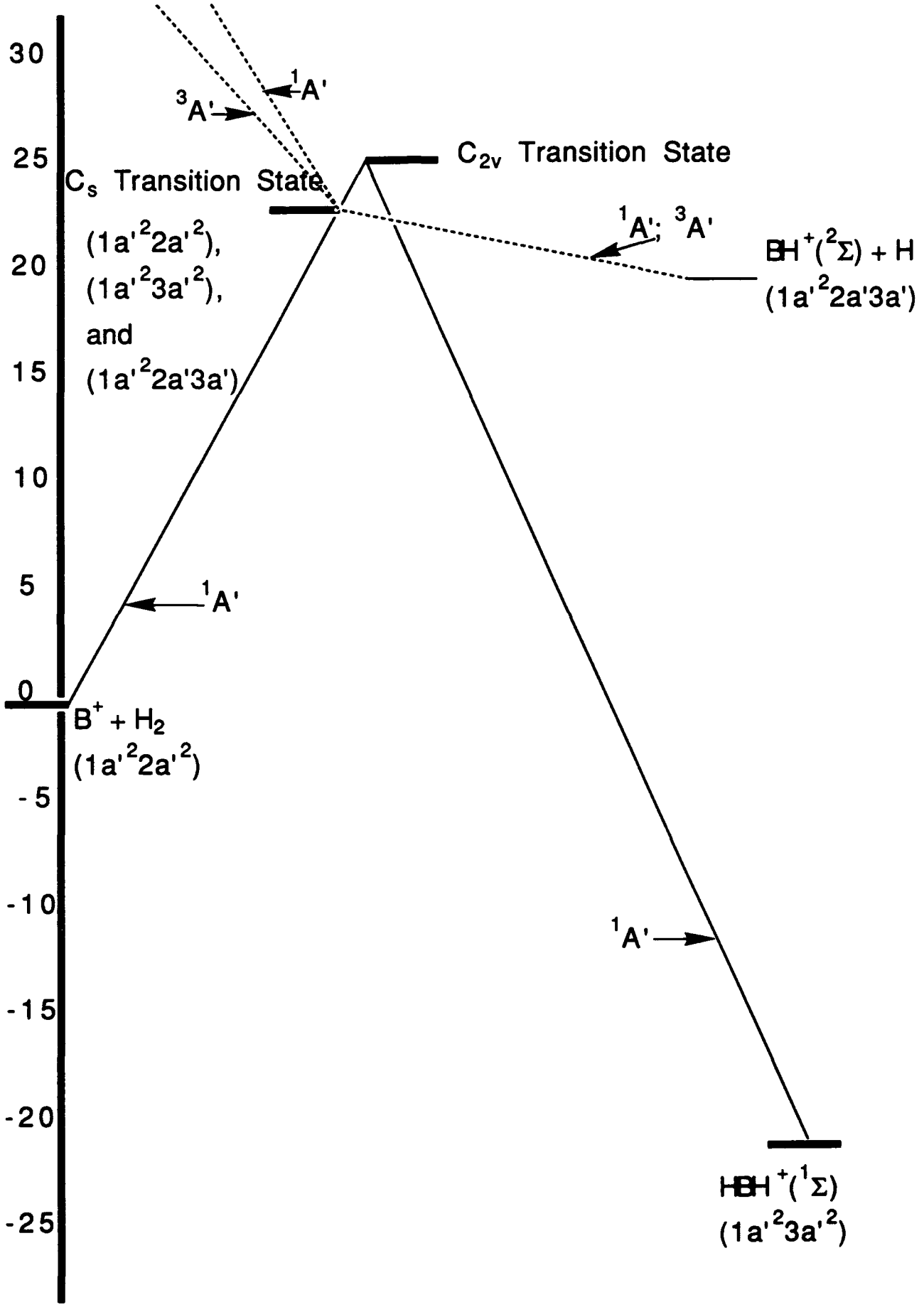
30
25
20
15
10
5
0
-5
-10
-15
-20
-25
$^1A'$
$^3A'$
C_{2v} Transition State
C_s Transition State
$(1a'^2 2a'^2)$,
$(1a'^2 3a'^2)$,
and
$(1a'^2 2a'3a')$
$^1A'$; $^3A'$
$BH^+(^2\Sigma) + H$
$(1a'^2 2a'3a')$
$^1A'$
$B^+ + H_2$
$(1a'^2 2a'^2)$
$^1A'$
$HBH^+(^1\Sigma)$
$(1a'^2 3a'^2)$

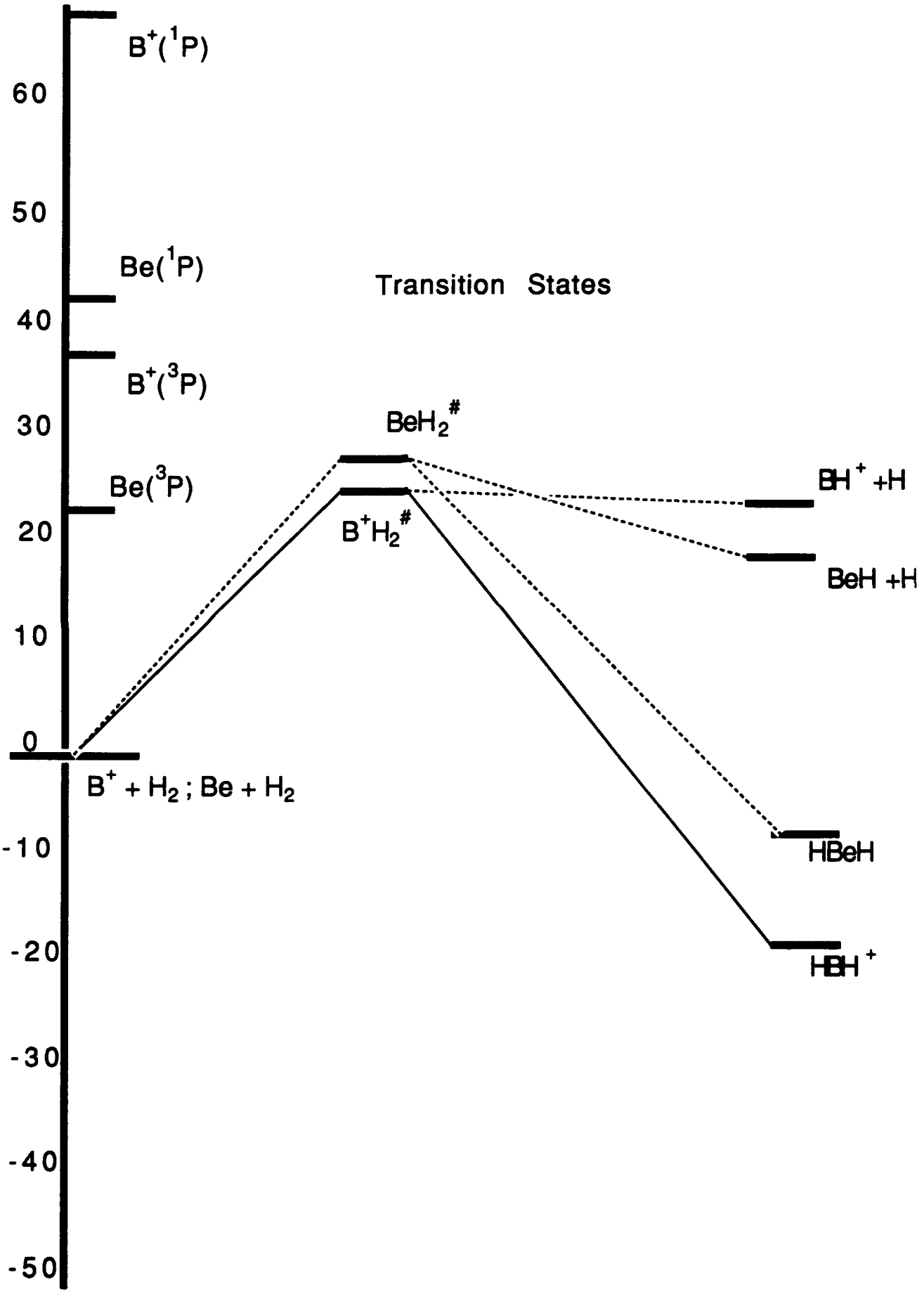
B+(1P)
60
50
Be(1P)
Transition States
40
B+(3P)
30
BeH2#
Be(3P)
BH+ +H
20
B+H2#
BeH +H
10
0
B+ + H2 ; Be + H2
-10
HBeH
-20
HBH+
-30
-40
-50